

UNIVERSIDADE ESTADUAL DE CAMPINAS  
SISTEMA DE BIBLIOTECAS DA UNICAMP  
REPOSITÓRIO DA PRODUÇÃO CIENTÍFICA E INTELLECTUAL DA UNICAMP

**Versão do arquivo anexado / Version of attached file:**

Versão do Editor / Published Version

**Mais informações no site da editora / Further information on publisher's website:**

<https://www.sciencedirect.com/science/article/pii/S2666032620300284>

**DOI: 10.1016/j.physo.2020.100041**

**Direitos autorais / Publisher's copyright statement:**

©2020 by Elsevier. All rights reserved.

DIRETORIA DE TRATAMENTO DA INFORMAÇÃO

Cidade Universitária Zeferino Vaz Barão Geraldo

CEP 13083-970 – Campinas SP

Fone: (19) 3521-6493

<http://www.repositorio.unicamp.br>



# Multipolar effects in the hysteresis behavior of 2D arrays of compass needles: Experiments and simulations

Murilo Ferreira Velo, Breno Malvezzi Cecchi, Fanny Béron, Kleber Roberto Pirota<sup>\*</sup>

*"Gleb Wataghin" Institute of Physics, University of Campinas, 13083-859, Campinas, SP, Brazil*



## ARTICLE INFO

Handling editor: Marcelo Knobel

### Keywords:

Magnetic multipoles  
Monte Carlo simulation  
Magnetic needles  
Magnetostatic interaction  
Multipole expansion

## ABSTRACT

Despite its easy experimental implementation, macroscopic systems composed of compass needles array show a rich and complex variety of physical phenomena that are not yet fully understood. In this work we consider the experimental realization of a square lattice of equally spaced millimeter sized compass needles, as well as its theoretical approach taking into account a proper higher order moments expansion of the magnetic potential, considering the actual shape of a compass needle. A Monte Carlo simulation, done using interaction energy value given by the previous expansion, showed excellent agreement with experimental results for the squared array magnetization process. Rather than the unique commonly considered dipolar contribution, the results evidence the importance of multipole expansion in considering interactions among magnetic elements with finite size, attributing to the magnetic particle shape a critical importance that could raise higher order contributions. In addition to the clear pedagogical relevance, the conclusions deserve attention, and reopen the discussion of whether dipolar interaction is the only relevant contribution to be considered in theoretical models in which magnetostatic interactions are important, e.g. superparamagnetic nanoparticles models.

## 1. Introduction

Magnetostatic interactions among magnets are the oldest magnetic manifestation that mankind has records of [1,2] and their important technological application dates back to 300–200 BCE, with the advent of the Chinese compass [1]. Despite having been known for a long time, the interest of the scientific community in its fundamental understanding and sophisticated practical applications has constantly increased. As it is widely known, the magnetic phenomena are present in many remarkable episodes of technological development: alternating current transformers, electric motors, electric generators, magnetic field sensors and data storage [3–5].

On the other hand, at the micro/nano world level, the magnetostatic interactions are always present, since there are at least two or more elemental magnets at a reasonable distance. For example, in paramagnetic materials, magnetostatic interactions are dominant and can explain the broadening of measured magnetic resonance lines [6]. In ferromagnetic materials, magnetostatic interactions play an important role determining the material magnetic domain structure [7]. In molecular magnets, due to the relatively large spin involved, dipolar, a particular case of general magnetostatic interaction, can play the

protagonist in determining the magnetic behavior [8]. Concerning superparamagnetic systems, most theoretical models that take interactions into account only pay attention to pure dipolar contribution though involved dimensions sign that special attention should be paid for higher order contributions as well [17].

In this regard, the possibility to build an array of macroscopic, but small, magnets, arranged in a specific periodic lattice, and study its behavior under external applied magnetic field, could bring us helpful information in the understanding of real systems, whether a crystal (for which the magnets are the elemental spins) or a huge amount of magnetic nanoparticles are concerned.

Several works are dedicated to emulate atomic elemental magnets using different macroscopic constituents like circular nanodots [9], single domain elongated islands [10,11], nanowires [12] and, more sympathetic, compass needles [13,14]. Despite its fundamentally different origin, the short-range exchange interaction responsible for intrinsic magnetic orders (ferromagnetism, antiferromagnetism, etc.) [15] can generate interesting magnetic configuration that can also be emulated, within certain limits, by an array of small magnets arranged in a specific geometrical configuration. A very interesting example is the famous ice rule respected by elemental spins arranged in a pyrochlore structure

<sup>\*</sup> Corresponding author.

E-mail address: [krpirota@unicamp.br](mailto:krpirota@unicamp.br) (K.R. Pirota).

<https://doi.org/10.1016/j.physo.2020.100041>

Received 27 July 2020; Received in revised form 26 August 2020; Accepted 27 August 2020

Available online 6 September 2020

2666-0326/© 2020 The Author(s). Published by Elsevier B.V. This is an open access article under the CC BY-NC-ND license (<http://creativecommons.org/licenses/by-nc-nd/4.0/>).

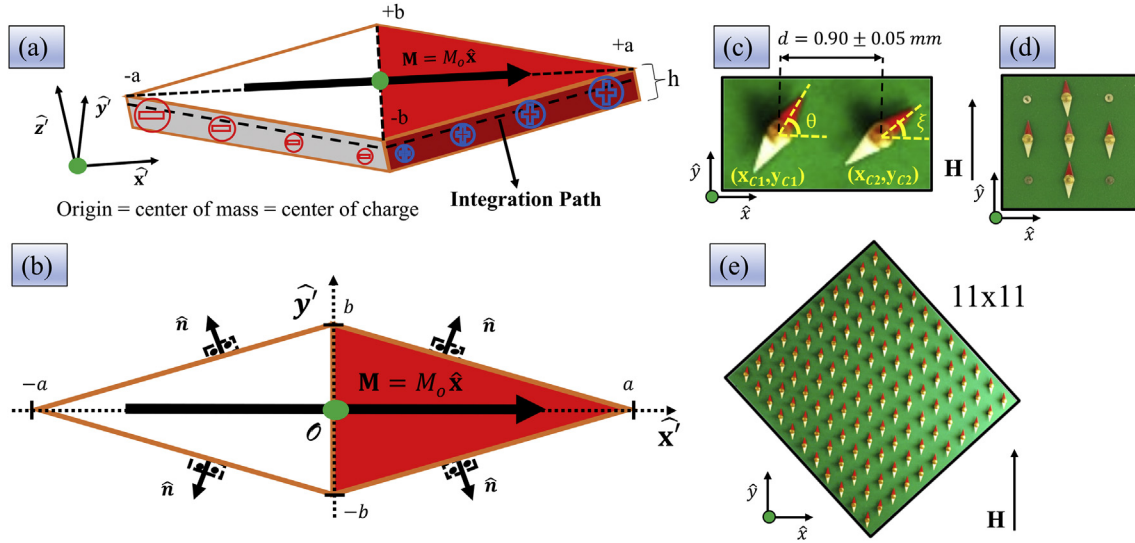


**Fig. 1.** Illustration of the rhombic compass needles and the studied arrays. (a) 3D perspective of the needle (major axis  $2a$  and minor axis  $2b$ ) with uniform magnetization pointing along  $x$  direction with constant magnitude ( $\mathbf{M} = M_0 \hat{x}$ ) and corresponding surface magnetic charge density. (b) Top view showing the needle boundary used for integration and the normal orientation  $\hat{n}$  of each needle section. (c) Simple system of two needles. (d) System of five needles in a cross arrangement. (e)  $11 \times 11$  square array.

present in the so-called spin ice materials [16]. In this regard, very interesting works have been published in the last 10 years, concerning the fabrication and study of static and dynamic magnetic properties of those artificial macro-spin arrays.

Arrays composed of magnetic islands with nanometric dimensions as individual magnetic elements (nanodots) [9,17] are an interesting option, but some difficulties come into play. Firstly, one must observe the temperature ranges that establish different magnetic situations: (i)  $T > T_{C1}$  (Curie temperature for the ferromagnetic nanodot itself), where the system exhibits a paramagnetic behavior and each nanodot is not a single domain particle at all; (ii)  $T_{C1} \geq T \geq T_{C2}$  (blocking temperature for a superparamagnetic system) where individual nanodots are in an ordered monodomain ferromagnetic phase but with thermal energy enough to overcome anisotropy barrier; and (iii)  $T < T_{C2}$ , still a ferromagnetic monodomain and showing a magnetostatic coupled phase (blocked regime). As the superparamagnetic blocking temperature is always below 80 K, the interesting coupled regime cannot be achieved at room temperature. Secondly, their small characteristic lengths, required to fulfill the monodomain condition, call for sophisticated magnetization measurements techniques like photoemission electron microscopy, available only in a few synchrotron facilities around the world.

The mentioned difficulties make the pedagogical system composed of small compass needles an interesting choice. Differently from nanodots, where the Zeeman effect due to external applied fields induce changes in the intrinsic magnetic moment direction of each island, in the case of magnetic needles, the field imposes a mechanical rotation of the needle as a whole.

Despite interesting different information given by each previously cited experimental work, they all assume the same fundamental physical approach, treating the individual magnetic entities as pure magnetic dipoles. Nevertheless, recent works show us that considering each island as a pure dipole and taking into account only the dipole-dipole interaction is not sufficient to explain the magnetic state patterns. In order to have a more realistic approach, we need to take into account the geometry of the nanostructures (e.g., dots, squares, ellipses, etc) and also the higher moments of the multipole expansion for the magnetic potential, which means, for example, to consider quadrupolar and octopolar terms in the expansion [9,18].

In this work, we give a model for the macroscopic magnetic needles which can lead to a better interface between the nano and the macro

magnetic system. The experimental system consists of a board with magnetic compass needles assembled on top of non-magnetic tips and free to rotate in 2D. The board was mounted inside a Helmholtz coils pair with a photographic camera on top, which produces images of the system configuration for a specific applied magnetic field. From the theoretical point of view, we performed a Monte Carlo simulation (MCS) taking into account higher magnetic multipole moments, up to order  $l = 5$ . The simulation allowed us to calculate  $\mathbf{M} \times \mathbf{H}$  curves and further compare them with the experimental ones. Using a simple two needles system as a starting point, the required parameters for the MCS were determined. Moving forward, bigger systems of five needles and  $11 \times 11$  needles arranged in a square lattice were considered, giving a real grasp of the importance of considering higher order multipolar contributions to theoretical models concerning interactions among small magnetic elements with finite size.

## 2. Methods

This section is divided into four parts: (1) experimental setup description of the needles and array configurations; (2) multipole expansion: the basis for a more realistic physical description; (3) energy landscape: interactions between two magnetic charge distributions; and (4) the Monte Carlo simulation.

### 2.1. Experimental setup

Our systems were composed of macroscopic rhombic compass needles with the following dimensions: major axis  $2a = (0.80 \pm 0.05)$  mm, minor axis  $2b = (0.30 \pm 0.05)$  mm and thickness  $h = (0.06 \pm 0.05)$  mm, as can be seen in Fig. 1 (a). To maximize the coupling among magnets, we chose a center-to-center distance  $d = (0.90 \pm 0.05)$  mm (Fig. 1(c)). The compass needles were placed on top of thin tips and were free to rotate around their centers. Three arrangements were investigated: a simple two needles system (Fig. 1(c)), five needles in a cross arrangement (Fig. 1(d)), and an  $11 \times 11$  square array (Fig. 1(e)). The experiments were performed in a quasistatic regime, subjecting each array to a magnetization cycle with magnetic field applied by a Helmholtz coil and constrained to the  $xy$  plane of the arrays (Fig. 1(c)–(e)).

In order to observe the orientation of each needle along the hysteresis, it was used a photographic camera (CANON 450D EOS, with 18–55

**Table 1**

Non-vanishing multipole moments  $Q_{l,m}$  (in units of the surface charge density  $\rho_M = \frac{\mu_0 M_0 b}{\sqrt{a^2 + b^2}}$ ) up to  $l = 5$  for the magnetic needle illustrated in Fig. 1(a). To obtain the multipoles with  $m > 0$ , use the identity  $Q_{l,-m} = (-1)^m Q_{l,m}^*$ .

	$m = -1$	$m = -3$	$m = -5$
$l = 1$	$\sqrt{2}a^2h$		
$l = 3$	$\frac{a^2h(-3a^2 - b^2 + 2h^2)}{4\sqrt{3}}$	$\frac{\sqrt{5}a^2h(a-b)(a+b)}{4}$	
$l = 5$	$\frac{a^2h}{8\sqrt{30}}(10a^4 + 2b^4 - 5b^2h^2 + 3h^4 + 2a^2b^2 - 15a^2h^2)$	$\frac{a^2h}{24}(5a^4 + 3b^4 - 5b^2h^2 + 3h^4 + a^2b^2 + 5a^2h^2)$	$\frac{\sqrt{7}a^2h}{8}(a^2 - b^2)^2$

mm f5.6/3.0 CANON LENS) that took top view photos of the array with 12 M pixels resolution. The integrated system (Helmholtz coils and photographic camera) was connected, via GPIB communication protocol, to a personal computer in which a LabVIEW program controlled the harmonious functioning, linking a configurational picture to the respective magnetic field value. To ensure a quasistatic regime, the program established an interval of 2 min between subsequent photos and magnetic field values.

An image pattern recognition was performed in order to acquire, in an automated way, the center position of each needle ( $x_c, y_c$ ) and their orientation angle (see Fig. 1(c)). For this purpose, a MatLab program, oriented by the contrast between the needles and a green background, cut out the needle image returning the mentioned parameters. Performing these procedures for all needles and for each magnetic field value, one ends up with the normalized hysteresis loop as well as the equilibrium configurations required for the intended study.

## 2.2. Multipole expansion

We performed multipole expansions, up to a certain maximum order  $l_{\max}$ , of the magnetic potential generated by the collections of needles. The spherical multipole moment of order  $l$  and secondary number  $m$  of a general surface magnetic charge distribution  $\sigma(\mathbf{r}')$  is defined by (see Ref. [19]):

$$Q_{l,m} = \int_S (r')^l Y_{l,m}^*(\theta', \varphi') \sigma(\mathbf{r}') d\mathbf{r}', \quad (1)$$

where  $Y_{l,m}(\theta, \varphi)$  are the spherical harmonics and the integration runs over the surface  $S$  in which the magnetic charges are distributed. Notice that the set of multipole moments of order  $l$ ,  $\{Q_{l,m}\}$ , has  $2l+1$  components with  $m = -l, -l+1, \dots, l-1, l$ . An important hypothesis, to ensure the uniqueness of the expansion, is the spatial coincidence of both center of mass  $\mathbf{r}_{\text{CM}}$  and the center of charge distribution  $\mathbf{r}_{\text{CC}}$ , which we can set at the origin for simplicity:

$$\mathbf{r}_{\text{CM}} = \mathbf{r}_{\text{CC}} = \frac{\int_S \sigma(\mathbf{r}') d\mathbf{r}'}{\int_S |\sigma(\mathbf{r}')| d\mathbf{r}'} = 0. \quad (2)$$

The magnetic charge distribution  $\sigma_M(\mathbf{r}')$  of a needle with magnetization  $\mathbf{M} = M_0 \hat{\mathbf{x}}$  (as in Fig. 1(a)) is

$$\sigma_M(\mathbf{r}') = \mathbf{M}(\mathbf{r}') \cdot \hat{\mathbf{n}}(\mathbf{r}'), \quad (3)$$

where  $\hat{\mathbf{n}}(\mathbf{r}')$  is the unit vector normal to the needle's surface (Fig. 1(a)–(b)). As a result, the magnetic charges concentrate only at the lateral surfaces. With the aid of two relevant symmetry properties presented by the charge spatial distribution,  $\sigma_M(\pi - \theta, \varphi + \pi) = -\sigma_M(\theta, \varphi)$  and  $\sigma_M(\theta, \varphi) = \sigma_M(\theta, \varphi + \pi)$ , one can calculate the multipole moments of the needle from Eq. (1):

$$\begin{aligned} Q_{l,m} &= \frac{1}{2} \left[ \int_C (r')^l Y_{l,m}^*(\theta', \varphi') \sigma_M(\mathbf{r}') d\mathbf{r}' + \int_C (r')^l Y_{l,m}^*(\pi - \theta', \varphi' + \pi) \sigma_M(r, \pi - \theta', \varphi' + \pi) d\mathbf{r}' \right] \\ &= \frac{[1 + (-1)^l]}{2} \int_C (r')^l Y_{l,m}^*(\theta', \varphi') \sigma_M(\mathbf{r}') d\mathbf{r}' \\ &= \frac{1 + (-1)^l}{2} \frac{1}{2} \left[ \int_C (r')^l Y_{l,m}^*(\theta', \varphi') \sigma_M(\mathbf{r}') d\mathbf{r}' + \int_C (r')^l Y_{l,m}^*(\pi - \theta', \varphi' + \pi) \sigma_M(r, \pi - \theta', \varphi' + \pi) d\mathbf{r}' \right] \\ &= \frac{[1 + (-1)^l]}{2} \frac{[1 + (-1)^m]}{2} \int_C (r')^l Y_{l,m}^*(\theta', \varphi') \sigma_M(\mathbf{r}') d\mathbf{r}'. \end{aligned} \quad (4)$$

We note, from Eq. (4), that the only non-vanishing moments are the ones with odd values for both  $l$  and  $m$ , shown in Table 1 up to  $l = 5$ .

The normalized moments  $Q_{l,m}/Q_{1,1}$  as a function of the needle aspect ratio  $h/a$  are shown in Fig. 2. The dashed line indicates our experimental compass needles. As an example, in our experimental case,  $Q_{3,1}$ ,  $Q_{3,3}$ ,  $Q_{5,1}$ ,  $Q_{5,3}$  and  $Q_{5,5}$  are at least 20% of the dipole moment  $Q_{1,1}$ , showing the importance of considering them in more accurate models.

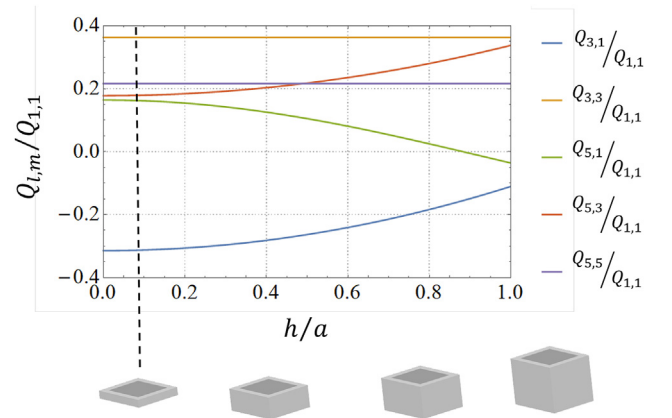


**Fig. 2.** Normalized non-vanishing multipole moments  $Q_{l,m}/Q_{1,1}$  for  $l = 3$  and  $l = 5$  as a function of the needle aspect ratio  $h/a$ . The dashed line indicates the aspect ratio for the experimental needles used in this work.

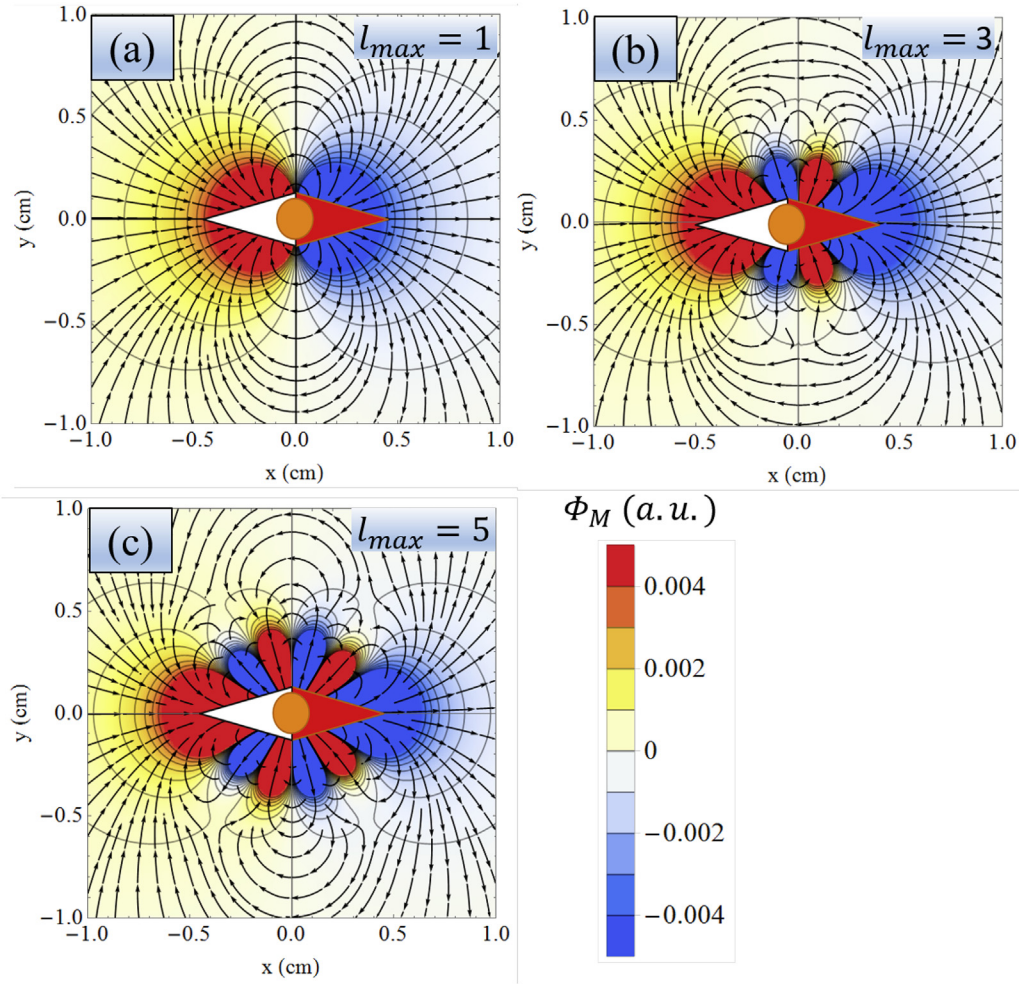


**Fig. 3.** Magnetic potential  $\Phi_M$  and magnetic field lines calculated considering the multipole expansion of a needle up to the order (a)  $l_{\max} = 1$ , (b)  $l_{\max} = 3$  and (c)  $l_{\max} = 5$ .

An interesting way to visualize the presence of terms with order above dipole is plotting the magnetic potential and the field lines, as done in Fig. 3. For the case of  $l_{\max} = 1$  (Fig. 3(a)) the magnetic field lines resemble most textbooks concerning magnets field lines, since they are of a dipole. However, for  $l_{\max} = 3$  and  $l_{\max} = 5$ , the magnetic field lines near to the needle substantially differ from those of a dipole mainly due to the magnetic charge distribution, which follows the needle geometry.

### 2.3. Magnetic potential energy

The potential energy  $E_{AB}$  between two localized magnetic charge distributions  $A$  and  $B$  separated by  $\mathbf{R}_{AB} = \mathbf{r}_B - \mathbf{r}_A$ , where  $\mathbf{r}_A$  and  $\mathbf{r}_B$  are the centers of charge of each distribution, is (see Ref. [19])

$$E_{AB} = \frac{\mu_0}{4\pi} \sum_{\substack{(l_A, m_A) \\ (l_B, m_B)}} T_{l_A, m_A; l_B, m_B}(\mathbf{R}_{AB}) Q_{l_A, m_A}^A Q_{l_B, m_B}^B, \quad (5)$$

where  $Q_{l_A, m_A}^A$  and  $Q_{l_B, m_B}^B$  are the multipole moments of each magnetic charge distribution and  $T_{l_A, m_A; l_B, m_B}(\mathbf{R}_{AB})$  is a geometric interaction tensor given by

$$T_{l_A, m_A; l_B, m_B}(\mathbf{R}_{AB}) = (-1)^{l_B} T_{l_A + l_B, m_A + m_B}^*(\mathbf{R}_{AB}) \times \sqrt{\frac{(l_A + l_B - m_A - m_B)!(l_A + l_B + m_A + m_B)!}{(l_A - m_A)!(l_B - m_B)!(l_A + m_A)!(l_B + m_B)!}}, \quad (6)$$

in which the dependence on  $\mathbf{R}_{AB}$  comes from the irregular normalized spherical harmonics  $I_{l,m}(\mathbf{r})$ ,

$$I_{l,m}(\mathbf{r}) = \sqrt{\frac{4\pi}{2l+1}} \frac{Y_{l,m}(\theta, \varphi)}{r^{l+1}}. \quad (7)$$

As a demonstration of how the model works, Fig. 4 shows the potential energy profiles, with  $l_{\max}$  up to 5 and  $H = 0$ , for two interacting needles with angular degrees of freedoms  $\theta$  and  $\xi$ . Fig. 4(a) shows the perfect dipole approximation, presenting energy minima for  $(\theta, \xi)$  equal to  $(0, 0)$  and  $(\pi, \pi)$ , and maxima for  $(0, \pi)$  and  $(\pi, 2\pi)$ . Fig. 4(b)–(d) show the influence of the higher orders terms of the expansion, which do not change the extreme points of the dipolar case, but change the inter-peaks region topography, giving rise to new local minimum and maximum peaks or metastable equilibrium points that are not present in the dipole approximation.

### 2.4. Monte Carlo simulation

We performed MCS using Eq. (5) for the magnetic potential energy and with the multipole moments  $Q_{l,m}$  displayed in Table 1. In the presence of an external magnetic field  $\mathbf{H}$ , the total hamiltonian  $\mathcal{H}$  also includes a Zeeman contribution  $E_{\text{Zeeman}}$ :

$$\mathcal{H} = E_{AB} + E_{\text{Zeeman}}$$



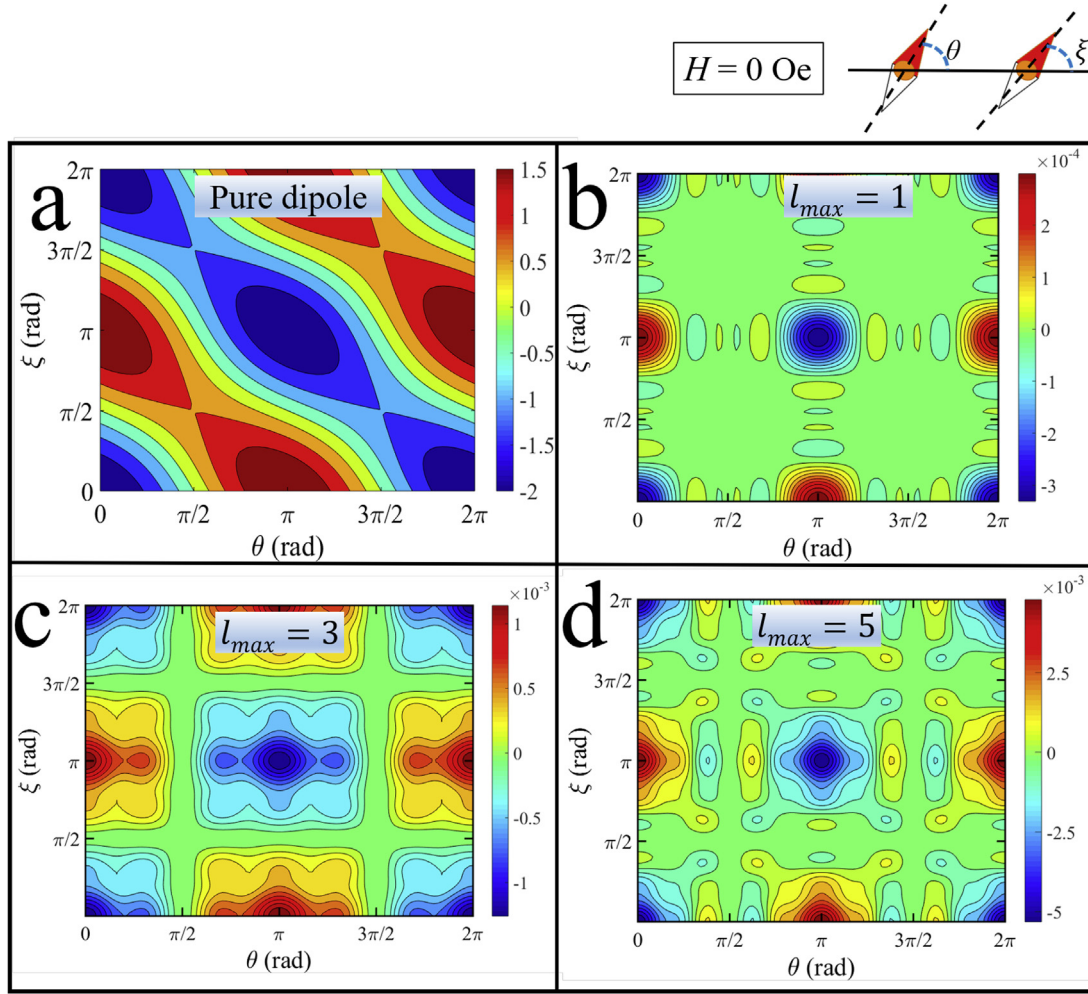


**Fig. 4.** Potential energy profiles of two needles with angular degrees of freedom  $\theta$  and  $\xi$ . (a) Pure dipole approximation, (b) multipole expansion for  $l_{\max} = 1$ , (c)  $l_{\max} = 3$ , and (d)  $l_{\max} = 5$

$$= \frac{\mu_0}{4\pi} \sum_{\substack{(l_A, m_A) \\ (l_B, m_B)}} T_{l_A, m_A, l_B, m_B}(\mathbf{R}_{AB}) Q_{l_A, m_A}^A Q_{l_B, m_B}^B - \mu_0 \mathbf{M}_A \cdot \mathbf{H} - \mu_0 \mathbf{M}_B \cdot \mathbf{H}, \quad (8)$$

where  $\mathbf{M}_A$  and  $\mathbf{M}_B$  are the total magnetization of distributions A and B, respectively.

The simulation uses the Metropolis algorithm [20,21] to energy minimization, as follows: (i) calculates the total energy from Eq. (8) for a random initial state; (ii) generates a new random state from the previous one, where each needle at a time can vary its direction by  $d\theta = 27^\circ$ ; (iii) calculates the new total energy and (iv) accepts the new state if it has a lower energy and rejects it otherwise, following the acceptance rate  $w = 0.988$ , i.e., even for energy values greater than the previous state it can be accepted depending on a random number generator. These steps were repeated  $n = 100$  times, achieving an energy value  $E$  which was sampled  $s = 50$  times. This total sampling of  $N = n \times s = 100 \times 50 = 5000$  was sufficient to ensure the convergence of the energy associated with each hysteresis point for all cases considered in this work.

The MCS parameters  $d\theta$  and  $w$  were determined empirically from the situation with just two needles (see Fig. 5). The MCS calibration was performed varying the  $w$  and  $d\theta$  values until reaching the best agreement between experimental and simulated data ( $d\theta = \pm 27^\circ$  and  $w = 0.988$ ).

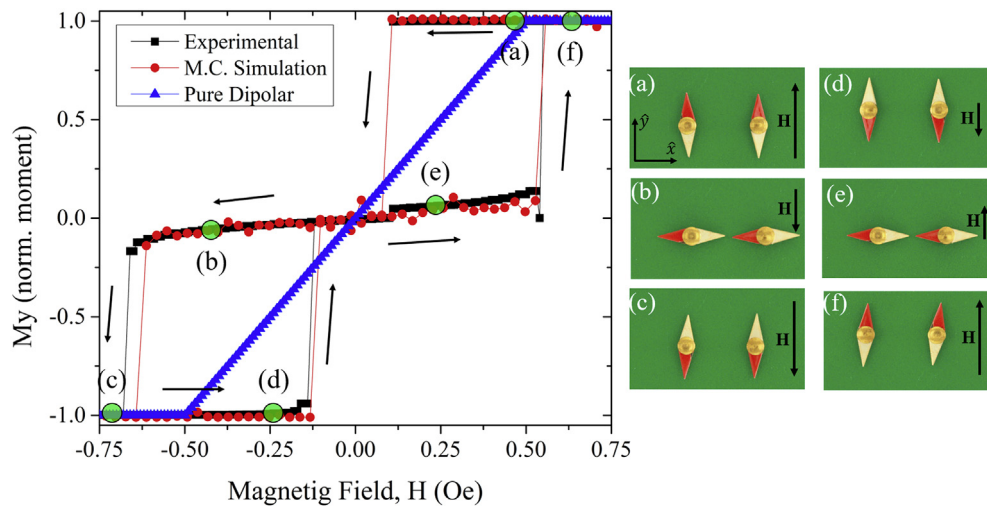
### 3. Results and discussion

Fig. 5 shows the results for the system of two needles subjected to a magnetization cycle. The experimental results (black curve of Fig. 5)

show the two needles initially pointing toward the magnetic field direction at the positive saturation ( $\uparrow\uparrow$ ). Decreasing the magnetic field we observe that, for  $H_{\text{switch},1} = 0.09$  Oe, the needles configuration changes from a ( $\uparrow\uparrow$ ) state (positive saturation) to a ( $\leftarrow\leftarrow$ ) state [ $(\rightarrow\rightarrow)$  also observed experimentally], representing a state configuration that remains stable until  $H_{\text{switch},2} = 0.72$  Oe, forming a plateau in the hysteresis loop. A symmetric path is followed if one starts with negative saturation and further increases the magnetic field.

As one can see, the pure dipole approximation (blue curve of Fig. 5) does not exhibit hysteresis and completely fails to describe the actual behavior. This fact can be attributed to the absence of local minima in its energy profile [see Fig. 4(a)], where the magnetization configuration could be trapped. On the other hand, MCS considering the magnetic multipole expansion (red curve of Fig. 5) obtained a curve almost perfectly superposed with the experimental result, revealing itself as an adequate model to describe the arrangement of macroscopic magnetic compass needles. Note that the higher order moments introduces local minima in the energy profile [Fig. 4(d)]. The results obtained for this simple system helped us in the calibration for the proper MCS parameters ( $d\theta = \pm 27^\circ$  and  $w = 0.988$ ) used in the other systems simulated in this work.

As a step forward, we considered the board with five needles arranged in a cross fashion, whose results are shown in Fig. 6. The agreement between MCS and experiment is achieved in a high level of detail, showing hysteresis loops with two new plateau states [points (b) and (e) of the hysteresis shown in Fig. 6], if compared to the previous two needles case, as the field goes from positive to negative saturation and vice versa. The



**Fig. 5.** Hysteresis loops for the case of two needles with separation  $d = (0.90 \pm 0.05) \text{ mm}$  between needles' centers and applied magnetic field in the  $y$  direction. (a)–(f): Snapshots showing the magnetic needles' orientations in each respective point indicated in the hysteresis loop.

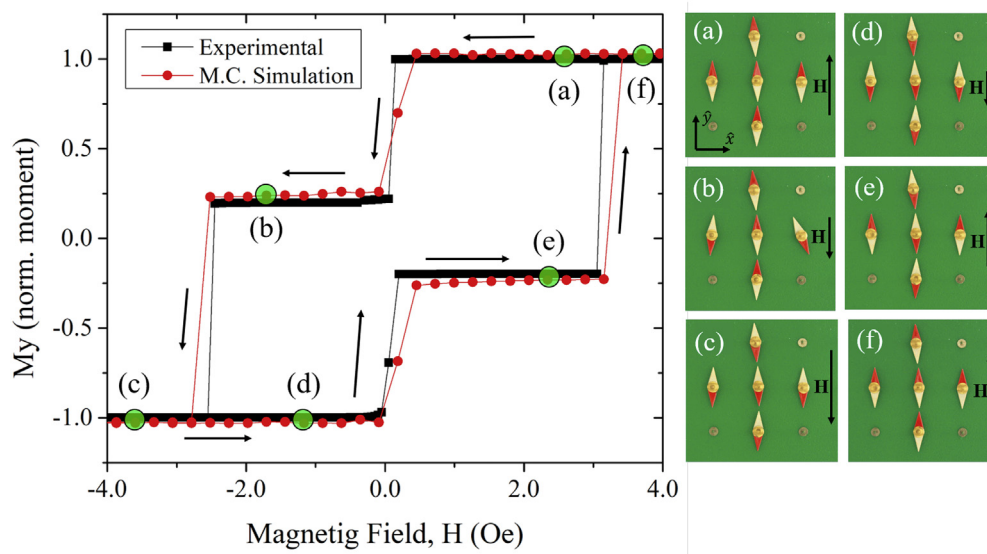


**Fig. 6.** Hysteresis loops for the case of  $n = 5$  needles in cross arrangement with separation  $d = 0.90 \pm 0.05 \text{ mm}$  between needles and applied magnetic field in the  $y$  direction. In (a)–(f) the array snapshots give the magnetic needle orientation in each respective state indicated in the hysteresis loop.

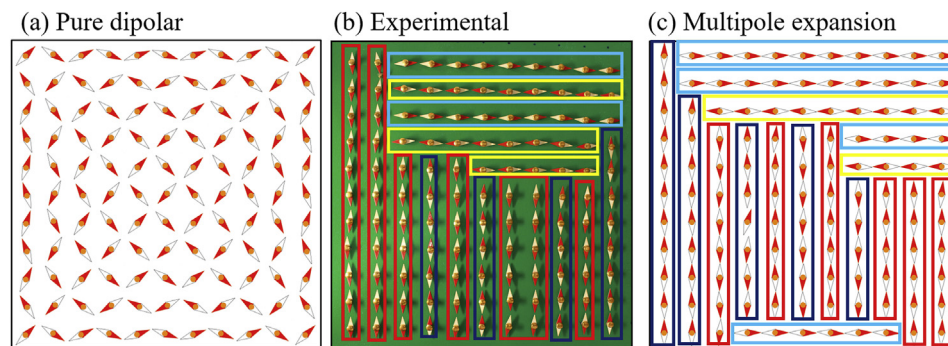


**Fig. 7.** (a) Ground state of an  $11 \times 11$  array of needles predicted by our Monte Carlo simulation considering only dipolar interactions. It shows a microvertex pattern. (b) Equilibrium state achieved by the experimental  $11 \times 11$  array showing line of needles pointing parallel either to  $x$  or  $y$  direction. (c) Ground state of an  $11 \times 11$  array of needles predicted by our Monte Carlo simulation considering multipole expansion up to  $l = 5$ . It shows lines of needles similar to the experimental case.

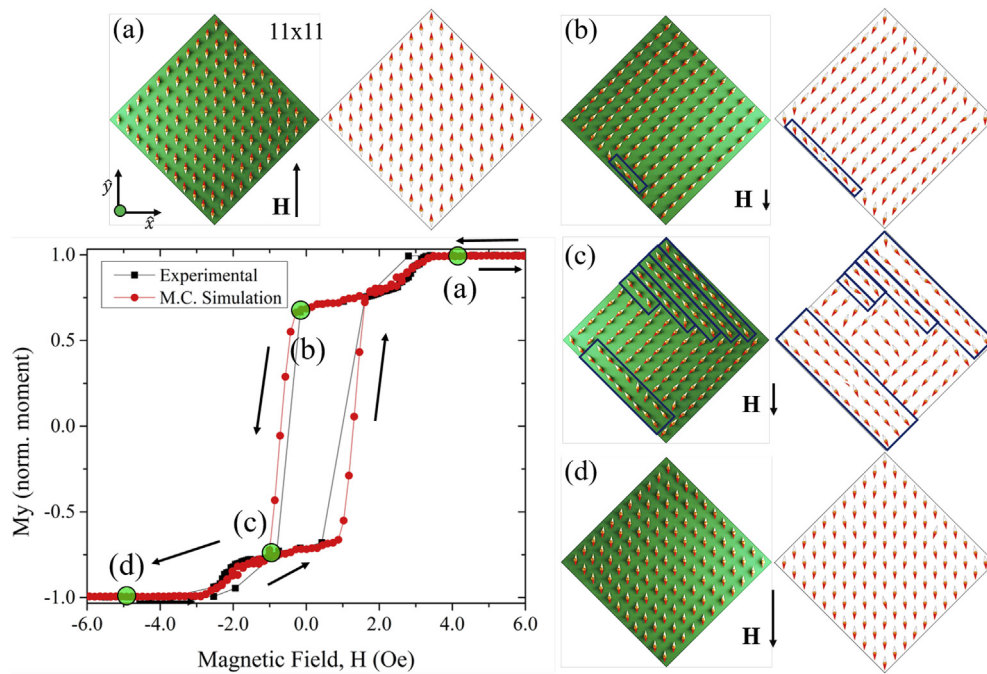


**Fig. 8.** Hysteresis loops for a square array with  $11 \times 11$  needles, with an applied magnetic field along one of the square's diagonal. (a)–(e): Snapshots showing the reversal mechanism for both experimental and simulated data.

photos enabled us to identify these additional states as created by the inversion of two lateral needles, as shown in Fig. 6(b) and (e).

For the square array system, its symmetry favors the magnetization alignment along the directions of the array's sides. For example, Fig. 7(b) shows the metastable state achieved after a magnetic field  $H \sim 5$  Oe was applied in a random elected direction and then abruptly switched off. Other possible metastable states for  $H = 0$  happened after application of the field along other arbitrary directions, but all of them showed similar lines of needles with same orientation. Olive et al. [13] also reported these magnetization lines feature for a  $22 \times 22$  experimental array. The authors verified that the ground state predicted by MCS considering only pure dipolar interaction exhibits a microvortex structure at the center and alternated lines formation at the edges, and therefore do not reproduce the experimental result. They were able to successfully reproduce it only by indirectly modeling the effect of the higher multipoles, in which they introduced an artificial anisotropic energy term which tends to stabilize the needles along  $x$  and  $y$  directions.

Indeed, the ground state of an  $11 \times 11$  array predicted by our MCS considering only dipolar contribution, shown in Fig. 7(a), also displays only a microvortex structure and no line formation, similar to the one predicted by Olive et al. On the other hand, the lines formation naturally emerges in our MCS when it considers explicitly higher multipole moments, as shown in Fig. 7(c), evidencing their proper contribution.

Finally, we also studied the  $11 \times 11$  squared array subjected to a magnetization cycle with magnetic field applied along one of the square's diagonal, which we set as the  $y$  direction. The results for both experiment and MCS are shown in Fig. 8 and the Supplementary Material includes videos showing the experimental and simulated system responses. As expected, for both positive and negative saturation configurations, the needles point parallel to the applied field according to the Zeeman energy minimization [Fig. 8(a) and (d)]. Starting from the positive saturation and decreasing the applied field, a coherent rotation of magnetic moments takes place, leading the system to a configuration in which all needles are pointing along  $[-1, -1]$  direction, except for a few needles at the edge [Fig. 8(b)]. The next shown state is reached after an abrupt step, where the magnetization decreases and the system goes to a metastable state with lines of needles pointing along both  $[1, -1]$  and  $[-1, -1]$  directions [Fig. 8(c)]. Finally, by means of a coherent rotation, the system goes to the

negative saturation, with all the needles pointing in  $-y$  direction [Fig. 8(d)]. We notice that the simulated MCS results agree with the experimental one, being expressive how good and realistic this fitting is.

#### 4. Conclusions

We demonstrated the importance of the multipole moments  $Q_{l,m}$  with  $l > 1$  on the behavior of several arrays of macroscopic compass needles subjected to quasistatic magnetic fields. In all cases, a good agreement between MCS and experiments required the consideration of these higher moments, specially for  $l = 3$  and  $l = 5$  which are just one order of magnitude below the dipole moment  $Q_{1,1}$ . Therefore, our results show that they are not all negligible, as opposed to what is usually assumed in most of the works in magnetism concerning systems of interacting extended magnets (artificial spin ices, superparamagnetic nanoparticles, etc). So, although we have discussed a relatively simple system using just classical magnetism, we open the debate, with a broad magnetism-related audience, on the importance of going beyond the dipole approximation to accurately describe general magnetic systems.

#### CRediT authorship contribution statement

**Murilo Ferreira Velo:** Methodology, Validation, Investigation, Writing - original draft, Writing - review & editing, Visualization. **Breno Malvezzi Cecchi:** Writing - review & editing, Visualization, Validation. **Fanny Béron:** Project administration, Supervision, Writing - review & editing. **Kleber Roberto Pirola:** Conceptualization, Supervision, Writing - original draft, Project administration, Funding acquisition.

#### Declaration of competing interest

The authors declare that they have no known competing financial interests or personal relationships that could have appeared to influence the work reported in this paper.

#### Acknowledgments

This work was supported by Conselho Nacional de Desenvolvimento e Científico e Tecnológico (CNPq); Coordenação de Aperfeiçoamento de



Pessoal de Nível Superior (CAPES); and Fundação de Amparo à Pesquisa do Estado de São Paulo (FAPESP – Grant 2017/10581-1).

## Appendix A. Supplementary data

Supplementary data to this article can be found online at <https://doi.org/10.1016/j.physo.2020.100041>.

## References

- [1] W. Lowrie, *Fundamentals of Geophysics*, second ed., Cambridge University Press, 2007 <https://doi.org/10.1017/CBO9780511807107>.
- [2] G.L. Verschuur, *Hidden Attraction: the History and Mystery of Magnetism*, first ed., Oxford University Press, 1996.
- [3] M.N. Baibich, J.M. Broto, A. Fert, F.N. Van Dau, F. Petroff, P. Etienne, G. Creuzet, A. Friederich, J. Chazelas, Giant magnetoresistance of (001)Fe/(001)Cr magnetic superlattices, *Phys. Rev. Lett.* 61 (21) (1988) 2472–2475, <https://doi.org/10.1103/PhysRevLett.61.2472>.
- [4] G. Binasch, P. Grünberg, F. Saurenbach, W. Zinn, Enhanced magnetoresistance in layered magnetic structures with antiferromagnetic interlayer exchange, *Phys. Rev. B* 39 (7) (1989) 4828–4830, <https://doi.org/10.1103/PhysRevB.39.4828>.
- [5] S.S.P. Parkin, M. Hayashi, L. Thomas, Magnetic domain-wall racetrack memory, *Science* 320 (5873) (2008) 190–194, <https://doi.org/10.1126/science.1145799>.
- [6] J.H. Van Vleck, The dipolar broadening of magnetic resonance lines in crystals, *Phys. Rev.* 74 (1948) 1168–1183, <https://doi.org/10.1103/PhysRev.74.1168>.
- [7] C. Kittel, Physical theory of ferromagnetic domains, *Rev. Mod. Phys.* 21 (1949) 541–583, <https://doi.org/10.1103/RevModPhys.21.541>.
- [8] R. Sessoli, D. Gatteschi, A. Caneschi, M.A. Novak, Magnetic bistability in a metal-ion cluster, *Nature* 365 (6442) (1993) 141–143, <https://doi.org/10.1038/365141a0>.
- [9] E.Y. Vedmedenko, N. Mikuszeit, H.P. Oepen, R. Wiesendanger, Multipolar ordering and magnetization reversal in two-dimensional nanomagnet arrays, *Phys. Rev. Lett.* 95 (2005) 207202, <https://doi.org/10.1103/PhysRevLett.95.207202>.
- [10] H.R. V, D. G, O. B, M. E, R.A. Fraile, N. F, H.L. J, B.H. B, Artificial kagome spin ice: dimensional reduction, avalanche control and emergent magnetic monopoles, *Phil. Trans. Math. Phys. Eng. Sci.* 370 (1981) 5767–5782, <https://doi.org/10.1098/rsta.2011.0538>, 2012.
- [11] A. Farhan, P.M. Derlet, L. Anghinolfi, A. Kleibert, L.J. Heyderman, Magnetic charge and moment dynamics in artificial kagome spin ice, *Phys. Rev. B* 96 (2017), 064409, <https://doi.org/10.1103/PhysRevB.96.064409>.
- [12] M. Vázquez, K. Pirota, M. Hernández-Vélez, V.M. Prida, D. Navas, R. Sanz, F. Batallán, J. Velázquez, Magnetic properties of densely packed arrays of Ni nanowires as a function of their diameter and lattice parameter, *J. Appl. Phys.* 95 (11) (2004) 6642–6644, <https://doi.org/10.1063/1.1687539>.
- [13] E. Olive, P. Molho, Thermodynamic study of a lattice of compass needles in dipolar interaction, *Phys. Rev. B* 58 (1998) 9238–9247, <https://doi.org/10.1103/PhysRevB.58.9238>.
- [14] R. Novak, J. Sinnecker, Macroscopic system for studies of magnetic dipolar interaction in small particles, *J. Magn. Magn. Mater.* 272–276 (2004) 1557–1558, <https://doi.org/10.1016/j.jmmm.2003.12.997>.
- [15] W. Nolting, A. Ramakanth, *Quantum Theory of Magnetism*, first ed., Springer Science & Business Media, 2009 <https://doi.org/10.1007/978-3-540-85416-6>.
- [16] S.T. Bramwell, M.J.P. Gingras, Spin ice state in frustrated magnetic pyrochlore materials, *Science* 294 (5546) (2001) 1495–1501, <https://doi.org/10.1126/science.1064761>.
- [17] N. Mikuszeit, E.Y. Vedmedenko, H.P. Oepen, Multipole interaction of polarized single-domain particles, *J. Phys. Condens. Matter* 16 (49) (2004) 9037–9045, <https://doi.org/10.1088/0953-8984/16/49/019>.
- [18] M. Ewerlin, D. Demirbas, F. Brüssing, O. Petracic, A.A. Ünal, S. Valencia, F. Kronast, H. Zabel, Magnetic dipole and higher pole interaction on a square lattice, *Phys. Rev. Lett.* 110 (2013) 177209, <https://doi.org/10.1103/PhysRevLett.110.177209>.
- [19] A. Stone, *The Theory of Intermolecular Forces*, second ed., Oxford University Press, 2013 <https://doi.org/10.1093/acprof:oso/9780199672394.001.0001>.
- [20] N. Metropolis, A.W. Rosenbluth, M.N. Rosenbluth, A.H. Teller, E. Teller, Equation of state calculations by fast computing machines, *J. Chem. Phys.* 21 (6) (1953) 1087–1092, <https://doi.org/10.1063/1.1699114>.
- [21] D.P. Landau, K. Binder, *A Guide to Monte Carlo Simulations in Statistical Physics*, fourth ed., Cambridge University Press, 2014 <https://doi.org/10.1017/CBO9781139696463>.